Tampere University

Metin Patli

STRUCTURAL CHARACTERIZATION OF NANOHOLES ON ALGASB SURFACE TO ESTIMATE DIMENSIONS OF GASB QUANTUM DOTS

Bachelor's Thesis
Faculty of Engineering and Natural Sciences
Examiner: Prof. Mircea Guina
April 2024

ABSTRACT

Metin Patli: Structural characterization of nanoholes on AlGaSb surface to estimate dimensions of GaSb quantum dots
Bachelor's Thesis
Tampere University
Bachelor's Programme in Science and Engineering
April 2024

Quantum dots (QDs) are used in applications such as quantum communication and quantum computing as single and entangled photon emitters. Due to their nanoscale dimensions, quantum confinement effects become pronounced. Hence particle in a box model is valid for such structures. This results in a direct correlation between optical properties and dimensions of a QD. Recently, GaSb QDs have been grown by filling nanoholes formed by local droplet etching (LDE). LDE is a two step method used for nanohole fabrication. Firstly, Al atoms are deposited on AlGaSb surface under small group V atmosphere to form Al droplets. Subsequently the sample is annealed in a small group V flux. At the end, nanoholes form in the AlGaSb surface. It is important to study dimensions of nanoholes formed by LDE which gives information about the QD dimensions formed by filling these nanoholes.

In this research work nanohole dimensions are studied using atomic force microscopy (AFM). The results show that increasing Al coverage in range θ_{Al} = 1.76-1.90 ML for droplet formation has an increasing effect on nanohole dimensions. The effect of increasing Al coverage on nanohole dimensions studied using two microscopy systems: Veeco Dimension 3100 and Veeco Dimension Icon. The results confirm that the dimensional data obtained from Veeco Dimension Icon is more reliable compared to data obtained from Veeco Dimension 3100.

Keywords: local droplet etching, atomic force microscopy, quantum dots, nanoholes, GaSb

The originality of this thesis has been checked using the Turnitin OriginalityCheck service.

PREFACE

I would like to thank my supervisor Abhiroop Chellu for his invaluable support during writing this thesis.

Tampere, 23 April 2024

Nursultan Metin Patli

CONTENTS

1.INTRODUCTION........ 1
2.METHODS........ 3
2.1 Local Droplet Etching (LDE)........ 3
2.2 Atomic Force Microscopy (AFM)........ 4
2.2.1 Introduction to AFM........ 5
2.2.2 Working principle........ 5
3.RESULTS........ 8
3.1 AFM Images from Veeco Dimension 3100........ 8
3.2 AFM Images from Veeco Dimension Icon........ 13
4.CONCLUSIONS........ 15
REFERENCES........ 16

LIST OF SYMBOLS AND ABBREVIATIONS

AFM	atomic force microscopy
Al	aluminium
AlGaSb	aluminium gallium antimonide
AlSb	aluminium antimonide
GaSb	gallium antimonide
LDE	local droplet etching
QD(s)	quantum dot(s)
Sb	antimony

1. INTRODUCTION

Quantum dots (QDs) are nanostructures which have dimensions comparable to exciton Bohr radius [1]. Due to the small size of the crystallite, quantum confinement effects become important [2]. As the crystallite size decreases, band gap energy will increase due to the increasing quantum confinement effect [1]. Band gap energy is the difference between valence band, occupied with electrons and conduction band, where electrons can move freely [3]. When electromagnetic radiation, having equal or higher energy than the band gap energy, is applied to such structure, it creates an electron-hole pair [4]. Recombination of an electron and a hole results in photon emission which has wavelength inversely proportional to the band gap energy [4]. In conclusion, the optical properties of a QD are directly correlated to its dimensions [1].

QDs can be used as single and entangled photon emitters [5], [6], [7]. Such structures also used in technology such as: quantum communication, quantum simulation, and quantum computing [2]. Therefore, QDs are an important research topic.

Fabrication of QDs can be achieved by several methods, such as Stranski−Krastanov growth, droplet epitaxy and filling nanoholes formed by local droplet etching (LDE) [7]. While in droplet epitaxy the QD structure form above the surface, in LDE process QDs are fabricated by filling nanoholes that are formed inside the substrate [8]. This will result in a direct correlation between nanohole dimensions and QD dimensions. Since the optical properties of QDs are directly correlated to QD dimensions, it is also directly correlated to nanohole dimensions. Therefore, it is important to study dimensions of nanoholes formed by LDE which gives information about optical properties of the QDs formed by filling these nanoholes.

In this thesis LDE method is used for fabricating the nanoholes. Experimental nanohole dimension results are obtained from atomic force microscopy (AFM) images. AFM is suitable for imaging nanoholes because it creates a 3D map of surface, and it has sub-nanometer resolution in vertical direction. The aim of this research is to give the most

accurate dimensional data of nanoholes with the help of AFM, which may help further research in developing gallium antimonide (GaSb) QDs.

2. METHODS

This chapter will give an overview of the LDE process as well as AFM working principle, its advantages, and limitations.

2.1 Local Droplet Etching (LDE)

To be able to understand nanohole formation mechanism, one needs to know the LDE process. LDE is a technique used in nanohole fabrication. Unlike droplet epitaxy, LDE method performed in higher temperatures and lower group V fluxes [7], [8]. Higher temperatures allow deep nanohole formations in the range 3-100 nm [9], [10]. The process parameters such as, group V flux and temperature have effect on nanohole dimensions [7], [10].

LDE process in this research work is carried out on an aluminium gallium antimonide (AlGaSb) surface which is grown on a GaSb substrate [7]. Etching process took place in a molecular beam epitaxy growth chamber. Etching starts with aluminium (Al) deposition under small group V atmosphere (Figure 1a) [7], [11]. After Al coverage θ_{Al} surpasses a critical coverage $\theta_{c,\,Al}$ droplet formation begins by following Volmer-Weber growth [7], [11]. Due to the minimization of surface energy, separate droplets formed on the surface [11]. Droplet formation terminated by closing the Al cell shutter.

After droplet formation, sample is annealed in a small group V flux (Figure 1b) [7], [11]. Antimony (Sb) flux can be adjusted accurately due to its low vapor pressure [7]. During the process, vapor Sb dissolves in Al droplet and meets with solid Sb. This causes nucleation at the triple-phase line where three phases of Sb meets [7]. Subsequently, solid form of Sb dissolves into droplet which results further nucleation [7]. As a consequence, droplet volume decreases and nanoholes with aluminium antimonide (AlSb) rings form (Figure 1c) [7]. The ring surrounding the nanohole is formed by Al atoms from the droplet along with Sb atoms from the vapor phase and substrate surface [7].

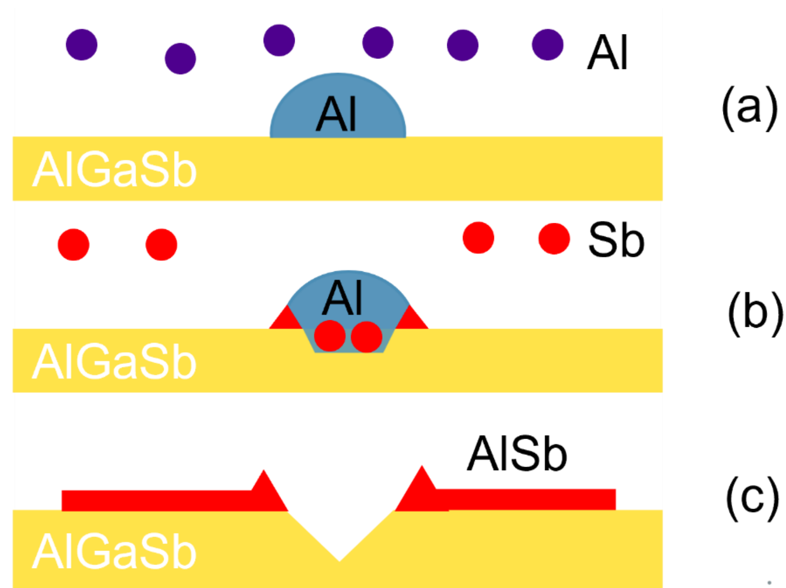

Figure 1. *Illustration of LDE process. (a) Etching starts with Al deposition. (b) It is followed by annealing under small group V flux. (c) At the end, nanoholes with AlSb rings form in the AlGaSb surface* ***[7]***

Nanohole dimensions can be controlled by changing process parameters such as temperature, Sb flux and Al coverage [7], [12]. As studied in previous research, for temperature range 570-680°C, nanohole dimensions increase while nanohole density decreases exponentially [12]. The research also shows that, for a studied range of increasing Al coverage values, density will first increase and then it saturates while depth and diameter will increase proportional to powers of 2/3 and 1/3 respectively [12]. Low Sb fluxes allow deep nanohole formation, however for lower temperatures more Sb is required for completing the etching process [7].

In conclusion, nanohole formation is a two-step process; droplet deposition and etching [11]. The size of the nanohole as well as the density can be adjusted by changing the initial droplet dimensions and droplet etching conditions.

2.2 Atomic Force Microscopy (AFM)

AFM is a type of scanning probe microscopy, invented in 1986 by Binnig and his coworkers [13]. Following sections will give an overview of AFM.

2.2.1 Introduction to AFM

AFM can be used for measuring stiffness, conductivity, magneticity as well as creating topography of a surface at nanoscale [14]. Due to its various modes, AFM can be applied in different fields, such as materials science, nanotechnology and biology [14]. In this research AFM is used for observing the dimensions of nanoholes with increasing Al coverage for droplet formation.

Optical microscopes use lenses which are diffraction limited by the laws of physics. In AFM, topological images are generated by scanning over a surface with using a sharp tip attached to a cantilever [14]. It creates a precise 3D surface map by studying the interaction between tip and sample's surface [14]. It has subnanometer resolution vertically and at most ~ 1 nm resolution laterally [14]. While scanning tunnelling microscopy can image only conducting samples, AFM can image all kind of samples [14], [15]. Additionally electron beam based techniques are not suitable for this research, since transmission electron microscopy is capable of creating a 2D surface map and one needs to predict depth maps from the given data when using scanning electron microscopy [16]. In this thesis depth values of nanoholes are also investigated which is the vertical distance calculated between surface and deepest point of the nanohole. AFM provides height data at each point in a 2D grid which makes it possible to investigate the shape of a nanohole structure, such as its depth and diameter.

2.2.2 Working principle

AFM has a working mechanism based on force measurements which is controlled by a feedback loop [14]. During imaging a sharp tip interacts with the surface at each point in a 2D grid [14]. When tip approaches surface cantilever bends [14]. Extended or compressed cantilever behaves like a spring and the force can be calculated by using Hooke's law [14]. The deflection of cantilever in vertical direction is used for force calculation [14]. Cantilever deflection is monitored by projecting a laser beam onto the photodiode above the tip [14].

One could ask the question; how does AFM define the height values? It keeps the force felt by the cantilever almost constant during scanning by changing its Z position with using a feedback loop [14], [17]. Before imaging begins, the parameters adjusted by the user to optimize the image quality. Such parameters include amplitude setpoint, integral gain and proportional gain. Amplitude setpoint is the amplitude of oscillation of

the cantilever set by the user and controlled during imaging by the feedback mechanism [18]. Integral gain and proportional gain related to each other by a ratio that may be different for distinct AFM systems [19]. Higher integral gain values enables AFM to track the surface topography more accurately while very high values result in noise in the imaging [19]. Proportional gain updates the error signal with given user specified value [20]. One could note that, compared to flat surfaces; rough surfaces, including surfaces with nanoholes, requires larger integral gain values [19]. As a summary, AFM defines height values with a feedback loop and optimization of the image quality achieved by setting image parameters before imaging begins.

AFM device has following main components; sample stage, a sharp tip attached to a cantilever, a laser, a detector, a photodiode, feedback electronics, a computer and piezoelectric scanners for adjusting XYZ positions of tip [14]. The positioning of piezoelectric scanners include some error, due to the reason it has hysteresis, nonlinearity and resonance [21]. Research shows that accuracy of piezoelectric scanner positions in lateral directions can be increased up to 1 nm [21].

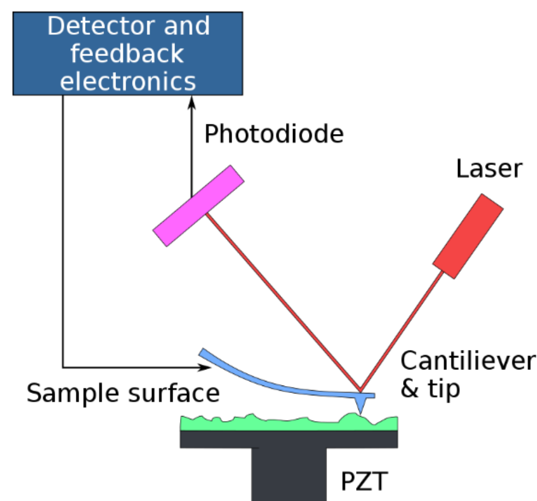

Figure 2. *Illustration of AFM* ***[22]***

AFM can be operated in several ways. Basic modes are contact modes and dynamic modes [23]. More advanced modes include single-dual pass methods, magnetic force microscopy, electrical AFM modes and electrochemical AFM [23].

In tapping mode, cantilever oscillates near or equal to resonance frequency [23]. Unlike contact mode, where tip is in steady contact with the surface, in tapping mode, or amplitude modulation mode, intermittent contact occurs [23]. This enables the tip to stay sharp during imaging [23]. In tapping mode, feedback parameter is amplitude of oscillation [23]. For a predefined amplitude setpoint value, feedback mechanism dynamically changes the Z-position of cantilever so that amplitude of oscillation stays constant [23]. The resulting height values are obtained from Z scanner [23].

As stated earlier, in tapping mode tip touches the surface rather than dragging across the surface [23]. For nanoholes, tapping mode is preferred as it less damages the surface compared to other methods. Additionally, tapping mode provides atomic resolution in vertical direction unlike contact modes [24]. In this research tapping mode is used for AFM imaging of nanoholes.

3. RESULTS

AFM results obtained from two different AFM systems: Veeco Dimension 3100 and Veeco Dimension Icon. Following chapters address data analysis techniques used in obtaining dimensional data from AFM images, the images obtained from AFM systems and effect of Al coverage on nanohole dimensions. In this research, the effect of increasing Al coverage on nanohole dimensions is studied.

3.1 AFM Images from Veeco Dimension 3100

In this thesis, five samples are studied, which have nanoholes on AlGaSb surface grown on GaSb layer. To study the effect of Al coverage on nanohole dimensions, the Al coverage value of samples set in increasing order. In Figure 3, one can see the 5×5 µm images obtained from AFM measurements.

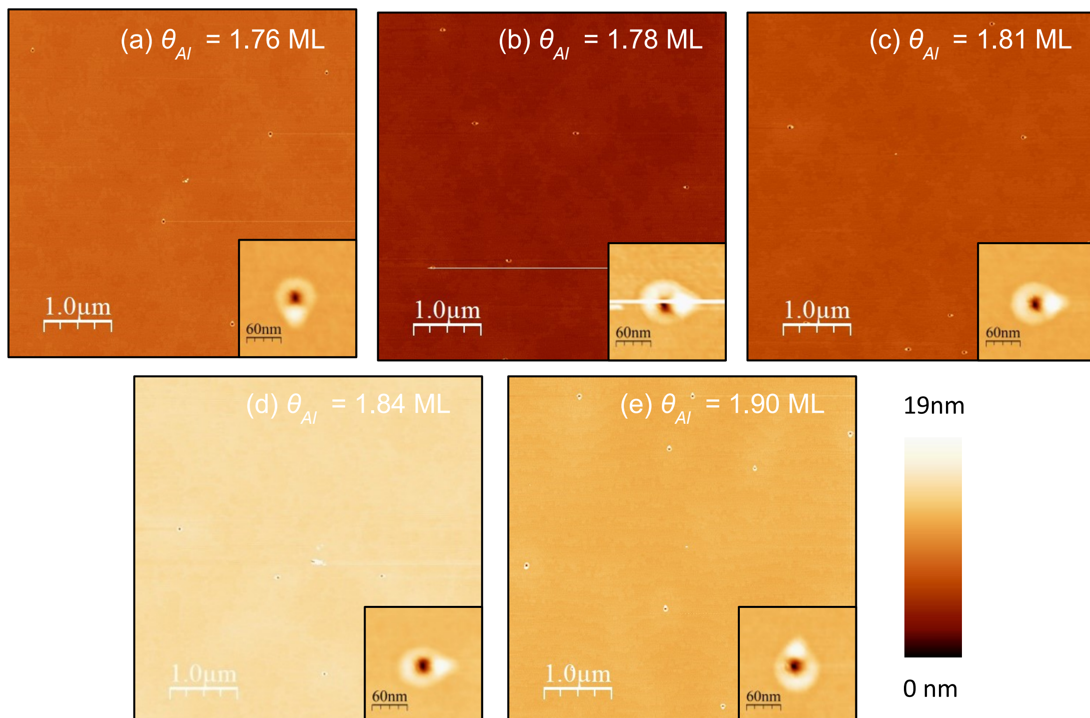

Figure 3. *5×5 µm AFM images of AlGaSb surface after LDE with deposition of Al range from 1.76-1.90 ML. Images show that increasing Al coverage has an increasing effect on nanohole diameters and depth values. Images (a), (c), (d) taken with 8 µm/s and (b), (e) taken with 10 µm/s tip velocity. Integral gain set to 0.2 V and proportional gain set to 0.4 V for all samples. The resolution used in imaging these pictures is 512×512 pixels/line. The zoomed nanohole images in the insets are 200×200 nm.*

After obtaining a 5×5 µm image, a 2×2 µm image (within the area of the 5×5 µm image) is taken for each sample. Imaging time depends on the resolution, image size as well as tip velocity [25]. One can express imaging time as $T=2NW/V_S$, where number of pixels (points) per line is N, image size is W×W and tip velocity is V_S [25]. Hence capturing a 2×2 µm and 5×5 µm image of a sample takes almost equal amount of time due to the chosen parameters. One can say that 2×2 µm images give more detailed information due to higher amount of data points in the same region. However, for estimation of nanohole dimensions one 2×2 µm image is not sufficient since it includes less amount of nanoholes. Hence statistics of nanohole dimensions are analyzed from 5×5 µm images. Figure 4 shows the 2×2 µm images obtained from AFM measurements.

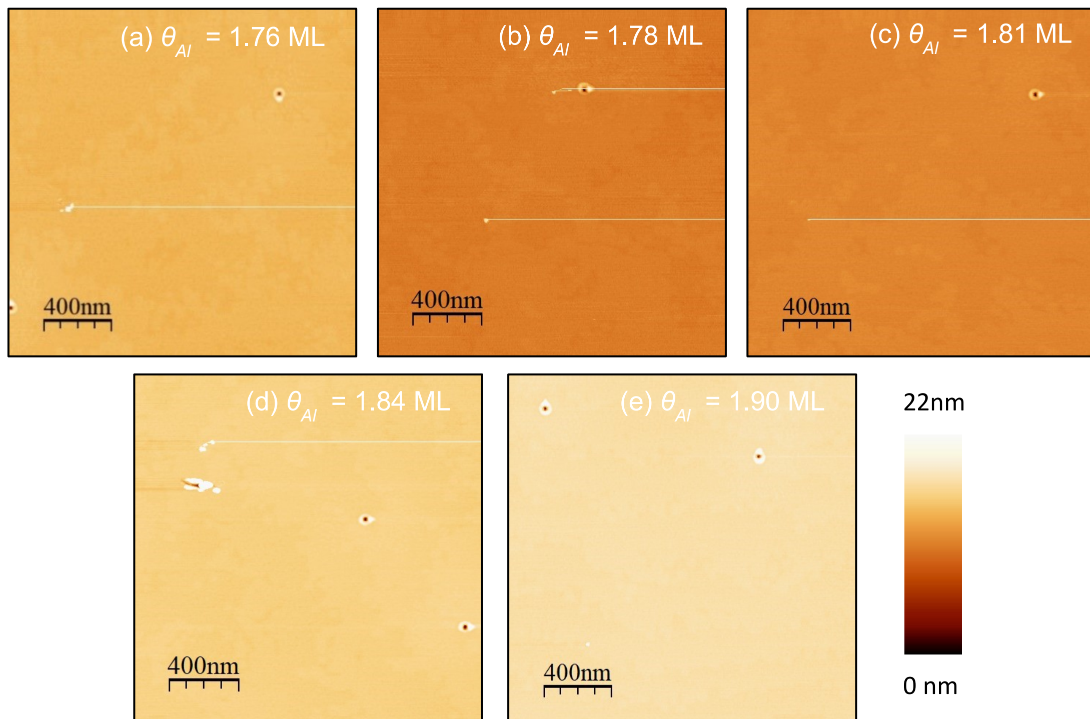

Figure 4. *2×2 µm AFM images showing a small portion of the 5×5 µm images shown in Figure 3. Images (a), (c), (d) taken with 3 µm/s, image (b) taken with 5 µm/s and (e) taken with 4 µm/s tip velocity. Integral gain set to 0.2 V and proportional gain set to 0.4 V for all samples. The resolution used in imaging these pictures is 512×512 pixel.*

Data analysis of nanoholes performed with the help of WSxM software [26]. The AFM images shown above includes height information. One can take a height profile in a specific direction (shown in Figure 5). Depth values can be calculated with taking height profile along any direction since the deepest point with respect to surface is same due to the flat nature of the surface. For investigating diameter values, height profiles taken

along two orthogonal directions: $\mathbf{01\bar{1}}$ and $\mathbf{0\bar{1}\bar{1}}$. For each direction, nanohole diameter calculated with using two different methods: finding the lateral distance between highest points and center of mass points of the ring. Figure 5 shows the illustration of the process followed during analysis of images.

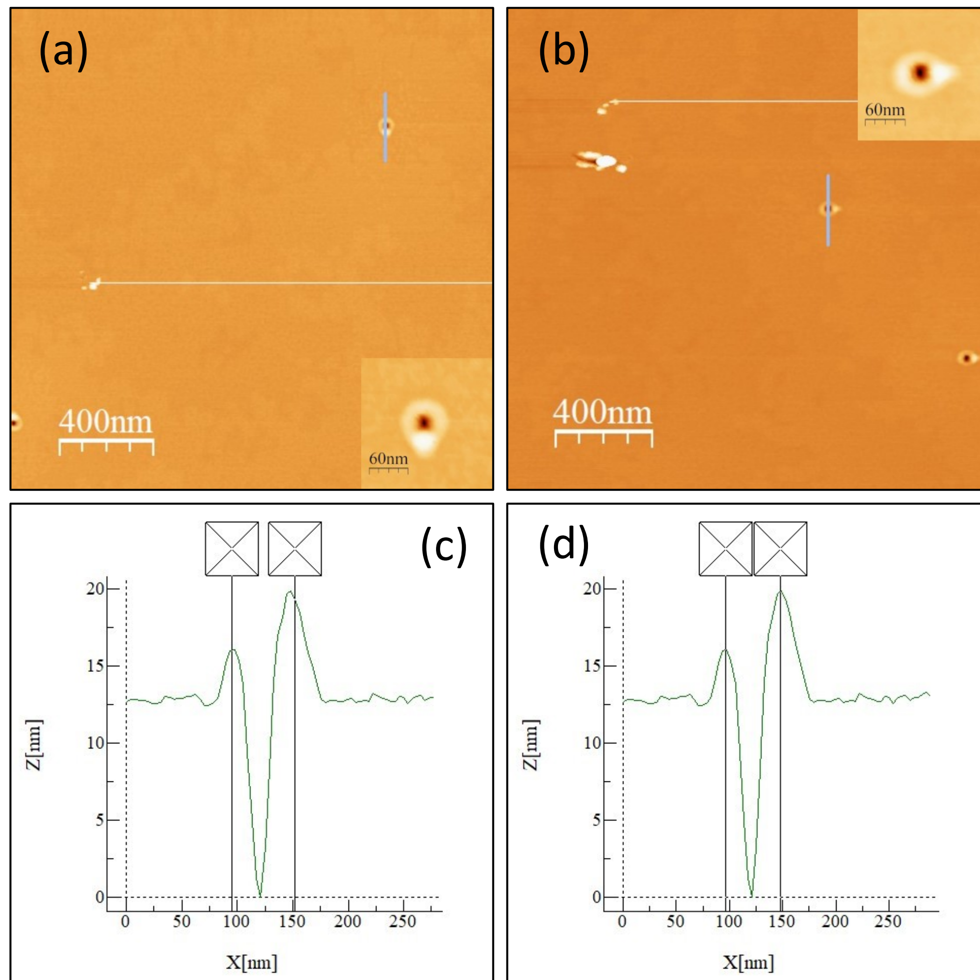

Figure 5. *Figures show the process followed doing data analysis of images shown in Figure 3 and Figure 4. Images (a) and (b) shows height profiles from* $\mathbf{01\bar{1}}$ *and* $\mathbf{0\bar{1}\bar{1}}$ *directions respectively. Along the* $\mathbf{01\bar{1}}$ *direction one can see a higher ring region compared to surrounding ring structure. Images (c) and (d) shows two methods for estimating nanohole diameter: from center of mass and top of the ring respectively. One can estimate nanohole dimensions from given figure: 12.5 nm for depth, ~51 nm for diameter measured from top and ~56 nm for diameter measured from center of mass.*

After performing data analysis of samples, mean values, and standard deviations for depth values of nanoholes calculated. Results from Veeco Dimension 3100 show a large error which may be due to AFM system, tip type or imaging parameters. Figure 6 shows the calculated depth values for 5×5 μm images.

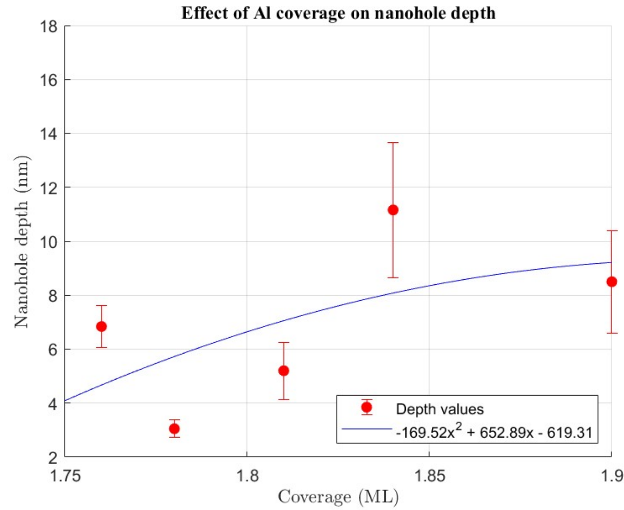

Figure 6. *Effect of increasing Al coverage on nanohole depth. Figure 3 data used in depth analysis.*

The mean values for diameters calculated considering four different cases (shown in Figure 7). Unlike depth, diameters measured along $\mathbf{01\bar{1}}$ direction from center of mass points and along $\mathbf{0\bar{1}\bar{1}}$ direction from maximum points of rings show an increase as Al coverage increases. Figure 7 shows the calculated diameter values for 5×5 μm images.

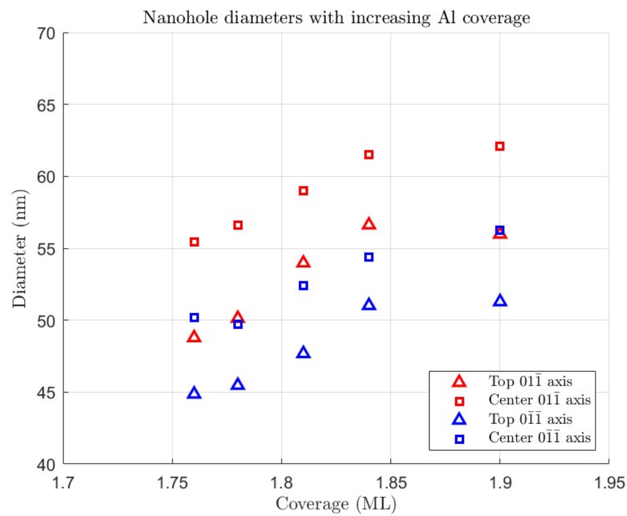

Figure 7. *Effect of increasing Al coverage on nanohole diameter. Figure 3 data used in diameter analysis. Diameter values measured from maximum locations of the rings (Δ) and from center of mass of the rings (□). The measurement directions are* $\mathbf{01\bar{1}}$ *(red) and* $\mathbf{0\bar{1}\bar{1}}$ *(blue).*

After analyzing depth values, sample shown in Figure 3 (b) investigated for a second time using Veeco Dimension 3100. The depth value is different from the same sample

imaged 1~2 months before. Same sample imaged with a different AFM system, Veeco Dimension Icon, and 9 nm average depth obtained which is approximately three times the value obtained with Veeco Dimension 3100. Subsequently, sample is imaged with Veeco Dimension 3100 with a new tip but the nanoholes don't resemble what is seen in Figure 3 (b). This is likely due to oxidation of the sample. The difference in results may be due to the contrast in AFM systems, and predefined imaging parameters in the two systems. Figure 8 shows the images obtained from two AFM systems for sample (b) shown in Figure 3.

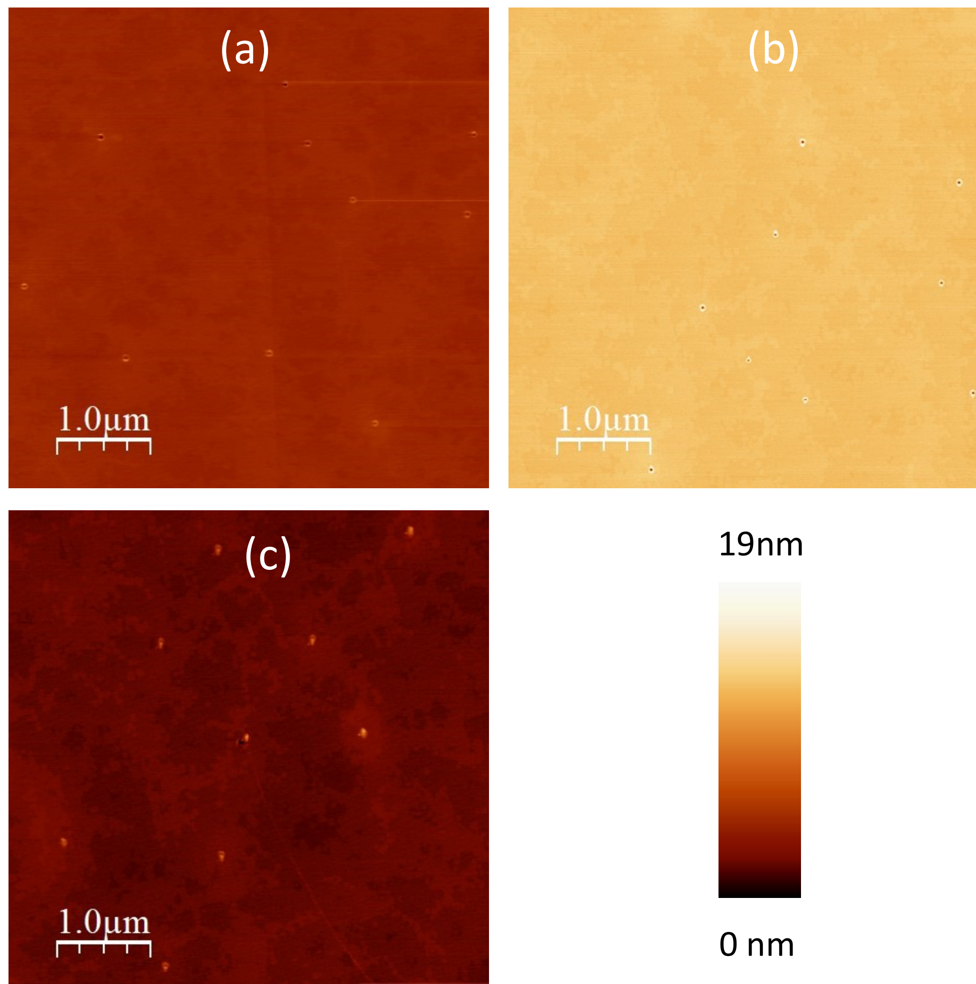

Figure 8. *5x5 µm AFM images of sample that has θ_{Al} = 1.78 ML shown in Figure 3. Image (a) captured 1~2 months after imaging the AFM image (b) indicated in Figure 3. Image (b) captured 8 days after imaging (a), and (c) captured 12 days after imaging (b). Pictures (a) and (c) obtained from Veeco Dimension 3100 while (b) obtained from Veeco Dimension Icon.*

By looking at the figures, one can say that diameter values show an increasing trend with increasing Al coverage. However, depth values have large error and Figure 8 shows that

it may be due to the AFM system used during imaging. In conclusion, there is need for imaging with Veeco Dimension Icon to get a more accurate dimensional data.

3.2 AFM Images from Veeco Dimension Icon

Due to the contrast observed in two AFM systems (shown in Figure 8) samples also imaged with Veeco Dimension Icon. To compare the two AFM systems only a 5×5 µm image taken for each sample. Below one can see the obtained AFM images.

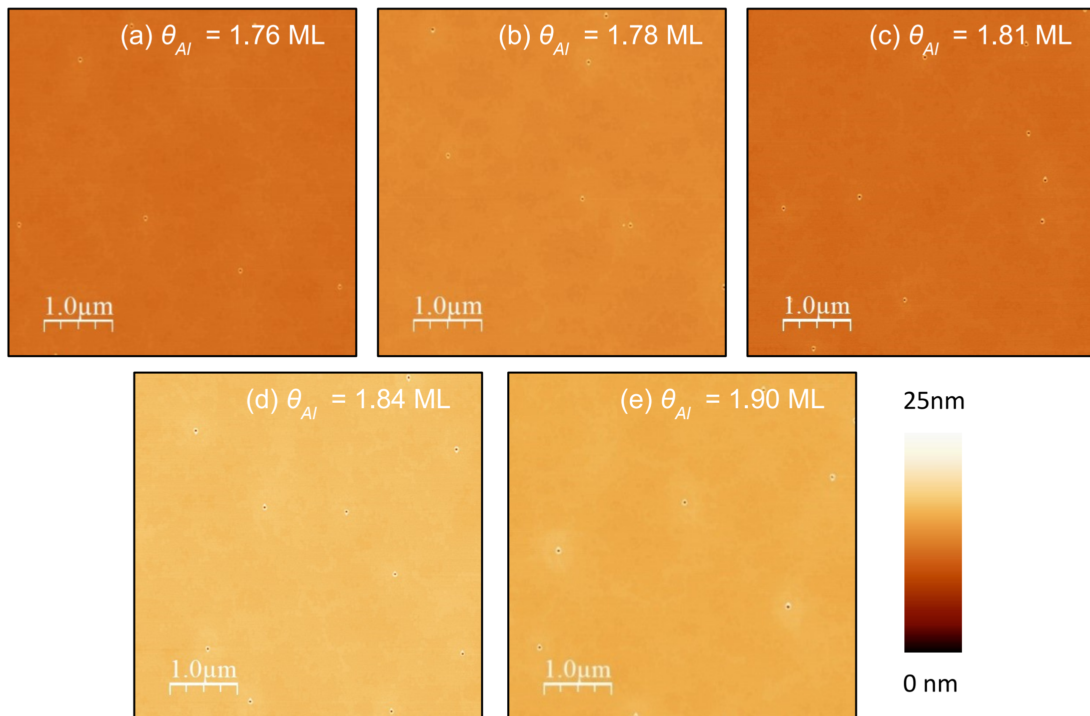

Figure 9. *5×5 µm AFM images of AlGaSb surface after LDE with deposition of Al range from 1.76-1.90 ML. Images taken with using 8 µm/s tip velocity. Integral gain set to 0.5 V and proportional gain set to 5 V for all samples. The resolution used in imaging these pictures is 512×512 pixel.*

Depth and diameter values calculated by following the same analysis technique (shown in Figure 5). Measured depth values show a clear contrast between two AFM systems. Figure 10 shows the calculated depth values for 5×5 µm images.

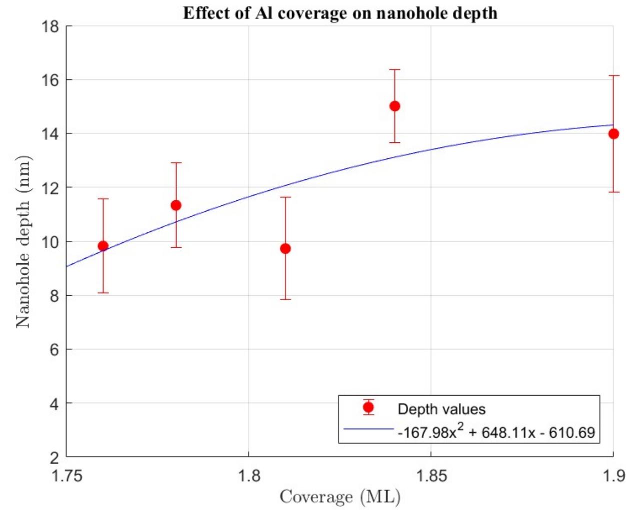

Figure 10. *Effect of increasing Al coverage on nanohole depth. Figure 9 data used in depth analysis.*

Unlike depth, measured diameter values show less variance when comparing two different AFM systems. The measurement results show an increase in nanohole diameter measured along $\mathbf{0\overline{1}\overline{1}}$ direction from maximum points of rings as Al coverage for droplet formation increases. Figure 11 shows the calculated diameter values for 5×5 μm images.

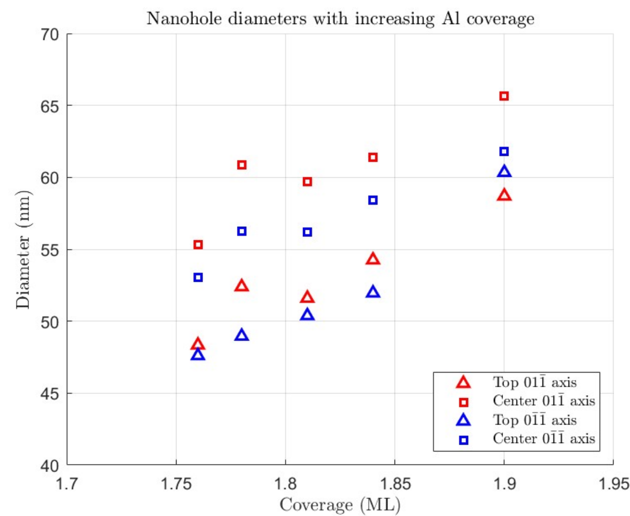

Figure 11. *Effect of increasing Al coverage on nanohole diameter. Figure 9 data used in diameter analysis. Diameter values measured from maximum locations of the rings (Δ) and from center of mass of the rings (□). The measurement directions are* $\mathbf{01\overline{1}}$ *(red) and* $\mathbf{0\overline{1}\overline{1}}$ *(blue).*

4. CONCLUSIONS

The results obtained from both AFM systems show an increase in nanohole dimensions as Al coverage for droplet formation increases. However, there is a large difference in depth measurements obtained from two different AFM systems. As discussed, during imaging with Veeco Dimension 3100 it has experienced that computed depth values change over different measurements. In conclusion, the results obtained from Veeco Dimension Icon is more reliable compared to the results from Veeco Dimension 3100.

Although the results show an increase in nanohole dimensions as Al coverage for droplet formation increases, it is just an estimate made from fitting models. To achieve a more accurate result one should analyze enough data points. In this research only one 5×5 μm image analyzed for each sample. However, one can take multiple images for one sample until a desired convergence to actual fitting model reached. Additionally, the image size can be reduced to get more precise results. In conclusion, by taking multiple images with a smaller image size for each sample one can get more accurate results.

To sum up, this research suggests increasing Al coverage on droplet formation in range θ_{Al} = 1.76-1.90 ML has an increasing effect on nanohole dimensions formed on AlGaSb surface grown on a GaSb layer based on the achieved results from two different AFM systems. A more accurate dataset would help in furthering research related to GaSb QDs.

REFERENCES

[1] F. W. Wise, “Lead Salt Quantum Dots: the Limit of Strong Quantum Confinement,” *Acc. Chem. Res.*, vol. 33, no. 11, pp. 773–780, Nov. 2000, doi: 10.1021/ar970220q.

[2] M. Gurioli, Z. Wang, A. Rastelli, T. Kuroda, and S. Sanguinetti, “Droplet epitaxy of semiconductor nanostructures for quantum photonic devices,” *Nat. Mater.*, vol. 18, no. 8, Art. no. 8, Aug. 2019, doi: 10.1038/s41563-019-0355-y.

[3] S. Khalifeh, “4 - OPTIMIZATION OF ELECTRICAL, ELECTRONIC AND OPTICAL PROPERTIES OF ORGANIC ELECTRONIC STRUCTURES,” in *Polymers in Organic Electronics*, S. Khalifeh, Ed., ChemTec Publishing, 2020, pp. 185–202. doi: 10.1016/B978-1-927885-67-3.50009-2.

[4] “Photons in Semiconductors,” in *Fundamentals of Photonics*, John Wiley & Sons, Ltd, 1991, pp. 542–591. doi: 10.1002/0471213748.ch15.

[5] Y. Arakawa and M. J. Holmes, “Progress in quantum-dot single photon sources for quantum information technologies: A broad spectrum overview,” *Appl. Phys. Rev.*, vol. 7, no. 2, p. 021309, Jun. 2020, doi: 10.1063/5.0010193.

[6] J. Lee, V. Leong, D. Kalashnikov, J. Dai, A. Gandhi, and L. A. Krivitsky, “Integrated single photon emitters,” *AVS Quantum Sci.*, vol. 2, no. 3, p. 031701, Aug. 2020, doi: 10.1116/5.0011316.

[7] J. Hilska, A. Chellu, and T. Hakkarainen, “Nanohole Etching in AlGaSb with Gallium Droplets,” *Cryst. Growth Des.*, vol. 21, no. 4, pp. 1917–1923, Apr. 2021, doi: 10.1021/acs.cgd.1c00113.

[8] Ch. Heyn, A. Stemmann, and W. Hansen, “Nanohole formation on AlGaAs surfaces by local droplet etching with gallium,” *J. Cryst. Growth*, vol. 311, no. 7, pp. 1839–1842, Mar. 2009, doi: 10.1016/j.jcrysgro.2008.11.001.

[9] Zh. M. Wang, B. L. Liang, K. A. Sablon, and G. J. Salamo, “Nanoholes fabricated by self-assembled gallium nanodrill on GaAs(100),” *Appl. Phys. Lett.*, vol. 90, no. 11, p. 113120, Mar. 2007, doi: 10.1063/1.2713745.

[10] Ch. Heyn, A. Stemmann, R. Eiselt, and W. Hansen, “Influence of Ga coverage and As pressure on local droplet etching of nanoholes and quantum rings,” *J. Appl. Phys.*, vol. 105, no. 5, p. 054316, Mar. 2009, doi: 10.1063/1.3079789.

[11] C. Heyn, T. Bartsch, S. Sanguinetti, D. Jesson, and W. Hansen, “Dynamics of mass transport during nanohole drilling by local droplet etching,” *Nanoscale Res. Lett.*, vol. 10, no. 1, p. 67, Feb. 2015, doi: 10.1186/s11671-015-0779-5.

[12] Ch. Heyn, S. Schnüll, and W. Hansen, “Scaling of the structural characteristics of nanoholes created by local droplet etching,” *J. Appl. Phys.*, vol. 115, no. 2, p. 024309, Jan. 2014, doi: 10.1063/1.4861722.

[13] G. Binnig, C. F. Quate, and Ch. Gerber, “Atomic Force Microscope,” *Phys. Rev. Lett.*, vol. 56, no. 9, pp. 930–933, Mar. 1986, doi: 10.1103/PhysRevLett.56.930.

[14] G. Haugstad, *Atomic Force Microscopy: Understanding Basic Modes and Advanced Applications*. Newark, UNITED STATES: John Wiley & Sons, Incorporated, 2012. Accessed: Mar. 03, 2024. [Online]. Available: http://ebookcentral.proquest.com/lib/tampere/detail.action?docID=894402

[15] B. Ebersberger, A. Olbrich, and C. Boit, “Application of Scanning Probe Microscopy techniques in Semiconductor Failure Analysis,” *Microelectron. Reliab.*, vol. 41, no. 9, pp. 1449–1458, Sep. 2001, doi: 10.1016/S0026-2714(01)00187-1.

[16] T. Houben, T. Huisman, M. Pisarenco, F. van der Sommen, and P. H. N. de With, “Depth estimation from a single SEM image using pixel-wise fine-tuning with multimodal data,” *Mach. Vis. Appl.*, vol. 33, no. 4, p. 56, Jul. 2022, doi: 10.1007/s00138-022-01314-w.

[17] F. Ahimou, M. J. Semmens, P. J. Novak, and G. Haugstad, “Biofilm Cohesiveness Measurement Using a Novel Atomic Force Microscopy Methodology,” *Appl. Environ. Microbiol.*, vol. 73, no. 9, pp. 2897–2904, May 2007, doi: 10.1128/AEM.02388-06.
[18] “Set point in tapping mode - SPM.” Accessed: Mar. 27, 2024. [Online]. Available: https://myscope.training/SPM_Set_point_in_tapping_mode
[19] “Gains - SPM.” Accessed: Mar. 27, 2024. [Online]. Available: https://myscope.training/SPM_Gains
[20] “Z Feedback Loop.” Accessed: Apr. 04, 2024. [Online]. Available: https://www.nanophys.kth.se/nanolab/afm/icon/bruker-help/Content/SPM%20Training%20Guide/Z%20Feedback%20Loop.htm
[21] Y. Wang, S. Wu, L. Xu, and Y. Zeng, “A new precise positioning method for piezoelectric scanner of AFM,” *Ultramicroscopy*, vol. 196, pp. 67–73, Jan. 2019, doi: 10.1016/j.ultramic.2018.09.016.
[22] “Atomic force microscopy,” *Wikipedia*. Feb. 02, 2024. Accessed: Mar. 09, 2024. [Online]. Available: https://en.wikipedia.org/w/index.php?title=Atomic_force_microscopy&oldid=1202288565
[23] “AFM Modes and Theory — Introduction - Nanosurf.” Accessed: Mar. 11, 2024. [Online]. Available: https://www.nanosurf.com/en/support/history-and-background-of-afm
[24] A. Schirmeisen, B. Anczykowski, and H. Fuchs, “Dynamic Modes of Atomic Force Microscopy,” in *Springer Handbook of Nanotechnology*, B. Bhushan, Ed., in Springer Handbooks. , Berlin, Heidelberg: Springer, 2007, pp. 737–766. doi: 10.1007/978-3-540-29857-1_27.
[25] T. Ando, “High-Speed Atomic Force Microscopy (AFM),” in *Encyclopedia of Biophysics*, G. C. K. Roberts, Ed., Berlin, Heidelberg: Springer, 2013, pp. 984–987. doi: 10.1007/978-3-642-16712-6_478.
[26] I. Horcas, R. Fernández, J. M. Gómez-Rodríguez, J. Colchero, J. Gómez-Herrero, and A. M. Baro, “WSXM: A software for scanning probe microscopy and a tool for nanotechnology,” *Rev. Sci. Instrum.*, vol. 78, no. 1, p. 013705, Jan. 2007, doi: 10.1063/1.2432410.